

The effect

by Imam Setiaji Ronoatmojo

Submission date: 20-Aug-2024 06:06AM (UTC+0700)

Submission ID: 2434701352


File name: 030002_1_5.0126091.pdf (903.09K)

Word count: 6608

Character count: 35500

1 RESEARCH ARTICLE | JUNE 12 2023

The effect of effective stress on pore pressure and velocity relationship in tectonic mechanism

Imam Setiaji Ronoatmojo ; Muhammad Burhannudinnur; Grace Stephanie Titaley

 Check for updates

AIP Conference Proceedings 2598, 030002 (2023)
<https://doi.org/10.1063/5.0126091>



CrossMark

Downloaded from http://pubs.aip.org/aip/acp/article-pdf/doi/10.1063/5.0126091/17985115030002_1_5.0126091.pdf

AIP Advances

Why Publish With Us?

 25 DAYS average time to 1st decision	 740+ DOWNLOADS average per article	 INCLUSIVE scope
--	--	---

[Learn More](#)



The Effect of Effective Stress on Pore Pressure and Velocity Relationship in Tectonic Mechanism

Imam Setiaji Ronoatmojo^{1, a)}, Muhammad Burhannudinnur¹, Grace Stephanie Titaley²

¹ Faculty of Earth Technology and Energy, Universitas Trisakti, Jl. Kyai Tapa No.1, Jakarta 11440, Indonesia

² PT. Pertamina EP, Menara Standard Chartered No. 164, Lt 16, Jl. Prof. Dr. Satrio, Jakarta 12950, Indonesia

^{a)} Corresponding author: aji.rono@trisakti.ac.id

Abstract. Tectonic mechanism is well-known to implicate conditions influencing the dynamics of poroelasticity. This phenomenon is also associated with the role of loading factor, hence pore pressure is strongly affected by tectonic regimes. The study aims to evaluate the effect of effective stress on pore pressure and velocity relationship, particularly when the impact of the loading mechanism is not prevailing. The research data was originated from several wells in Rantau Field, North Sumatra Basin, Indonesia. This oil field is located in the transcurrent fault structural area, where thrust fault regime becomes deeper, and is assumed to be a strike-slip fault regime, obviously observed from seismic-magnetoteluric data interpretation. The log data, including sonic, resistivity and density were selected to accompany seismic data acquired in 1994, due to the fields actively producing property. Therefore, the initial and historical production data up to 2017 were coupled. The result shows an increment in pore pressure, following the water injection activity, which further triggers matrix bonding, and increases the velocity values. This phenomenon is not common on instances where there is a normal fault tectonic regime.

Keywords: effective stress, pore pressure, velocity, tectonic mechanism

INTRODUCTION

The relationship between elastic properties and porosity is an important topic of discussion. This is typically known as a dynamic factor, when considered in association with pore pressure, which changes with the surrounding external conditions. Moreover, pore pressure also impacts on the state of stresses, where a decline in hydrocarbon production increases the normal stresses, while water injection produces the opposite effect. Furthermore, rock compression resulting from the interaction between the porous materials and the interstitial fluid, induces a rise in pore pressure as fluid escape is prohibited. This phenomenon results in the dilatation of the matrix bonding and progressive deformation of the rock, indicating a greater compliance in drained rocks compared to the undrained variety [1]. The reduction of Young's modulus and an increase in Poisson's ratio shows the influence of fluids on the litology. Thus, the saturated forms are relatively more disfigured than the dry variants under similar stress conditions [2][3][4][5]. In addition, compressive strength and deformation modulus further decreases with reduced loading rate [6][7][8][9]. Subsequently, adjustments are made to the mechanical response by freely moving fluids. The transfer of any shear stress is not possible with fluid, because of the amount of pore pressure acting on the rock-frame, which is often implicated in the declining total normal stresses [10]. Also, pore pressure is known as one of the factors responsible for the decline in rock strength [11][12][13][14]. This study aims to evaluate the effect of stresses, generated by the tectonic mechanism, on the relationship between pore pressure and velocity. The tectonic mechanism in this case is possibly identified from the sovereignty of the maximum horizontal stress (S_H) to the vertical stress (S_v), while the loading mechanism is characterized by the dominance of vertical stress (S_v). In spite of this study has never been conducted, this research uses mechanical properties from log data of production wells which describe shallow tectonic regimes in Nangroe Aceh Darussalam. The area of interest lies within the northern part of Sumatra in NW-SE orientation, and it is parallel to the subduction zone. This zone is a convergence of two tectonic plates which well-known to collide with strain partitions to produce two main structural components, where the first appears perpendicular to the trench, manifested by folds and thrust faults on the accretionary prism, while

7 the second accommodates oblique convergent strike-slip fault parallel to the trench [2,3,4,5]. Enormous tectonic strength triggered major earthquakes of 9.0 M in Sumatra-Andaman (2004) and 8.6 M_w in Nias Island (2005), close to the sub-sea epicenter [6]. Meanwhile, the lateral fault system and the Sumatra fault zone counterbalance the trench parallel to the slope components of the convergence between Indo-Australia and Eurasia plates [7,8,9].

The effective normal or vertical effective stress (V), originally known as an effective stresses concept refers to the difference between total normal stresses and pore pressure. In addition, most pore pressure is predicted by expressing elastic wave velocity as a function of vertical effective stress (σ_e), produced by vertical impact acting on the solid rock matrix. This is further defined as the difference between the overburden pressure, S_v and the pore pressure, P_p . In relation to solid rocks, Terzaghi's equation is written as:

$$\sigma_e = S_v - \alpha P_p \quad (1)$$

12 where α is the ratio of the V fluid pressure to overburden stress effects on grain surface after the stress is applied to consolidated rocks. This poroelastic coefficient in Terzaghi's original equation was introduced to consider the fluid pressure effect on grain surface when it is applied to consolidated rocks. Generally, a value between 0.7 and 1.0 and predominantly around 0.8 has been reported.

This impact is due to the rock matrix and the fluid content in the pore space overlying the formation of interest at a specific depth. The overburden pressure value S_v referred to as an integral of density is written as:

$$S_v = g \int_0^z \rho(z) dz \quad (2)$$

4 ρ is the bulk density of the formation, as a function of depth, z , while g denotes gravity acceleration, where an empirical relation for the pressure from compression transit time was introduced by Eaton (1975) in accordance with Terzaghi (1943) [15][16]:

$$P_p = S_v - (S_v - P_{hy}) \left(\frac{\Delta t_n}{\tau} \right)^3 \quad (3)$$

P_p , S_v and P_{hy} respectively represent the formation, overburden and hydrostatic pressure, while Δt and (Δt_n) are the transit time obtained from seismic data and normal compacted pressure in shales.

Eaton's methods are predominantly used in thick shale-rich lithology, where overpressure is primarily due to disequilibrium compaction and in some petroleum basins despite the restrictions as a result of the inability to reflect tectonic effects. However this method is invalid unless the normal compaction trend is built for all interest depth. Also, because this method is inapplicable in geologically complicated areas, several porosity/depth trends were published to identify the relationship between the compaction of shale sediments and depth of burial in different sedimentary basins [17][18]. In addition, a decrease in effective stress generally leads to a decline in compaction rate (higher porosity), consequently resulting in overpressure and low rock velocity. Therefore, velocity is used as a proxy for porosity retention to predict overpressure, although depth is a poor means to measure the processes impinged on a sedimentary section through time [19]. Furthermore, diagenetic processes and basin sediment compaction is continued, provided the existence of porosity is sustained. Therefore, the depth of burial offers an incomplete basis for porosity evaluation [20][21].

8 Bowers presented a modification of Eaton's methods after considering the limitations of the original model. Based on the alterations, the exponent power n was substituted for the exponent power 3, describing the velocity sensitivity to differential stress. The value of n depends on the geological formation being investigated ($n > 3$). Also, as the exponent in equation 4 becomes greater than 3, the model is, thus, able to simulate the tectonic curves [22].

$$P_p = S_v - (S_v - P_{hy}) \left(\frac{\Delta t_n}{\tau} \right)^n \quad (4)$$

8 This equation was not used despite the tectonic or formation uplift, although a higher velocity in the loading curve leads to similar effective stress. The compressional velocity (V_p) and the effective stress (σ_e) have a power relationship in the loading stage:

$$V_p = V_m + A \left(\sigma_e^m \left(\frac{\sigma_e}{\sigma_e^m} \right)^{1/U} \right)^B \quad (5)$$

where U is the unloading parameter describing sediment plasticity and calibrated with local data practically ranging from 3 - 8 in unloading cases. In addition, σ_e^m is the maximum effective stress at the beginning of the unloading depicted by a rebound on the $V_p - V$ cross-plot, V_m is the compressional velocity at the mudline (usually 5000 ft/s). Meanwhile A and B are the parameters calibrated with offset velocity, against effective stress data.

This study used several data from Rantau Field, an oil production field located approximately 135 kilometers northwestward from Medan (North Sumatera basin, Indonesia). Also, this is a part of the Eurasian plate now separated from south-east Asia by Malacca strait and Indo-Australian oceanic plates. Furthermore, R-01 was the first well drilled by BPM and recently there are 566 wells. This field reached a peak production of 32,477 BOPD (oil), with the shallow zone producing 868 BOPD and 27.4 MMSCFD (gas) as of 1973, prior to the re-activation by water flooding activities [23]. The volcanic arc is located westward and associated with subduction zone as well as the Semangko Fault, a well-known huge structural zone with physiographic expressions, also termed Bukit Barisan. These physiographic uplifts occurred since Early Eocene to the present, with three deformations specifically pre-tertiary, tertiary and quaternary. Meanwhile, the objective of this study is Keutapang Fm. (Late Miocene – Early Pliocene) with thickness ranging from 700 m to 1500 m in East Aceh [24]. This is identified as a product of deltaic sedimentation, consisting of shale, interbedded with sandstone varying from fine sand to pebble conglomerate. Tertiary deformation is characterized by the appearance of transcurrent fault structure namely Simpang Kanan Monocline, in the same direction with pre-tertiary deformation and represented by anticline and syncline with NW-SE pattern. Moreover, some derivative of Simpang Kanan monocline exposed on the surface remain active today [25]. Figure 1 illustrates this structural complex.

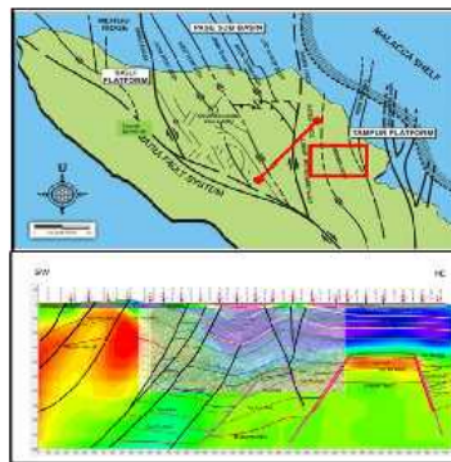


FIGURE 1. Site location (top) and overlaid seismic-magnetotelluric profile with SW-NE orientation (bottom).

MATERIALS AND METHODS

Kirsch method is employed to determine rock deformation. The wellbore stresses in terms of deformation, are assumed to be vertical and consist of the effective radial stress (σ_r), the effective axial stress (σ_z) and the effective circumferential stress (σ_θ) operating in a normal, parallel, and horizontal manner to the wellbore wall respectively, in addition, the circumferential stress acts orthogonal to σ_r and σ_z . Furthermore, rock strengths recognized from breakouts are designated by UC value, although hardly ever found in the drilling data. Ultimately the value is gained from previous empirical relations anytime the mud pressure is greater than pore pressure. The most important

issue while using well data is the alterations resulting from oil production and water flooding activities on pore pressure changes. This calculation was based on the following equation [26]:

$$\Delta P_z = \left[\frac{(\Sigma_{i=1}^n \frac{F_i}{n})_y - (\Sigma_{i=1}^n \frac{F_i}{n})_z}{(\Sigma_{i=1}^n \frac{F_i}{n})_x} \right] \quad (6)$$

Subsequently, there have been historical matching with reservoir simulation, where, the ratio of S_{hm} to pore pressure changes have been used to determine the change in porosity usually associated with the change of stresses. However, permeability is the strain dependent parameter [27]. Furthermore, the alterations to the pore pressure in the productive layers, initially computed in the fluid flow simulator, were used to calculate the updated state of stresses. Consequently, pressure change data were transferred to geomechanical simulator in order to accomplish a link for the computations. This worked iteratively as all parameters were matched. In addition, Navigator and ABACUS were used for reservoir and geomechanical simulator, respectively, while the algorithm for estimation have previously been discoursed in several papers [28][29][30][31].

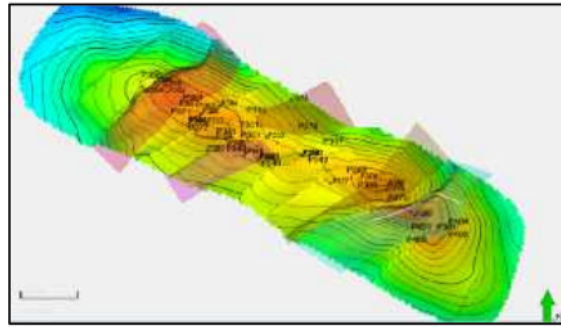


FIGURE 2. Structural map of this area with wells spread over alongside 3 major faults separating the region into compartments.

The sample wells are spread over Rantau structure, including part of the NW-SE ridge anticline, and are fragmented by the NE-SW oblique strike slip fault. These faults arrange a number of structural partitions and tend to seal or leak to the flowing fluid depending on the shale gauge ratio. Under these circumstances, a fault plane is unable to provide similar response to the reservoir continuity, and is influenced by the stress orientation and magnitude [32]. The magnitude also affects the increase rate of effective stress reflecting from K (bulk modulus) value, and therefore possibly modifies the V_p (P-wave seismic velocity) value. This phenomenon connects the principal stress magnitude with an important role in velocity and pore pressure relation.

RESULTS AND DISCUSSION

The results of several calculations on mechanical properties have been validated in this paper by the data obtained during drilling. This helps to discuss the effects of effective stresses on the relationship of pore pressure and velocity. In addition, the selected wells are positioned within the periodization category based on the seismic data conditions acquired in 1994. Subsequently, the mechanical properties are modeled in 3D, and the results, coupled with production data up to 2017, are finally updated. The intended effective stresses in this case are the difference between individual external principal stresses and pore pressure. External principal stresses possibly described as S_v exhibits strong influence on the loading mechanism or S_H , particularly on tectonics. However, the impact of modifications in effective stresses tends to affect the porosity and rock strength and causes a velocity change, based on the dynamic pore pressure. Furthermore, observations reported include pore pressure versus acoustic impedance, pore pressure versus velocity, velocity versus ($S_H - S_{hm}$), velocity versus ($S_H - S_v$), velocity versus ($S_H - P_p$), and velocity versus ($S_v - P_p$).

Pore Pressure

Pore pressure is significant in evaluating poroelasticity. The property dynamic is revealed as the pore pressure gradient values characterized by mud weight value reference. In addition, the occurrence of break out indicates the pore pressure was not balanced. According to the oil well P-404, a robust relationship between pore pressure and principal stresses with the nature of rock elasticity was established. This is represented by an increased UCS and elastic modulus to form a more rigid rock. Meanwhile, the enhanced pore pressure value originated from the rise in total gas content leading to a narrow mud weight window and a drilling break. Overall 1D estimation is confirmed by each event in the drilling record containing parameters, including W (weight of bit) and R (rate of penetration). Subsequently, the results from calculations are only applied after provisions based on the actual conditions are fully achieved.

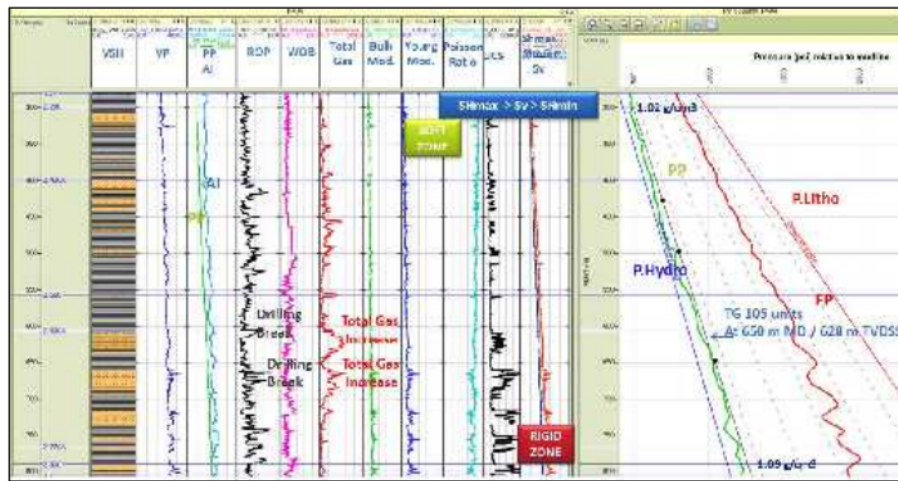


FIGURE 3. Pore pressure and mechanical properties based on log data and validated by drilling events.

Further analysis refers to the data within the period of seismic data acquisition, known to support the kriging process. However, pore pressure distribution was attained after several iterations. Moreover, there is a close relationship between pore pressure and porosity distribution, and it is obtained from seismic inversion. Both distributions are controlled by the orientation of the NE-SW trending structure caused by 2 factors: sedimentation and deformation. In addition, the magnitude is particularly determined by its tectonic regime from Z-600 horizon slicing. The Z-600 is recognized as a reservoir zone in the strike-slip fault regime after the cross-over between S_{H1} and S_b , and the curve intersects at a depth of approximately 400 - 450 m. These changes are very significant to analyze in this study. The modifications are the primary reason influencing the relationship between pore pressure and velocity, and therefore, are not solely affected by loading mechanism. Furthermore, there are no other tectonic mechanisms such as clay mineral diagenesis or H (high pressure high temperature) conditions in this field. This is represented in Fig. 4, where an increase in density corresponds to higher velocity, although there is a separate trend for shale and reservoir. Moreover, the separation of reservoir and non-reservoir is based on a cut-off value of 0.65. Sand reservoir was observed with scattered data or higher uncertainty, according to the crossplot of R and V_p . This is probably not caused by Keutapang sandstones, also classified as lithic arenites originating from Barisan mountain terrain. Keutapang sands are sand-rich delta system that prograde north-west. Meanwhile, the shale consistency is due to the lower and stable deposition energy compared to sandstone. The shale linearity trend emphasized that the compaction process gradually occurred in the delta system owned by all well data. In addition, the homogeneity shows a real impact within 1D pore pressure estimation, as a result of the N (normal compaction trend) predicted along the shale tendency from the sequence. This is clearly defined from the sonic or resistivity trend [33].

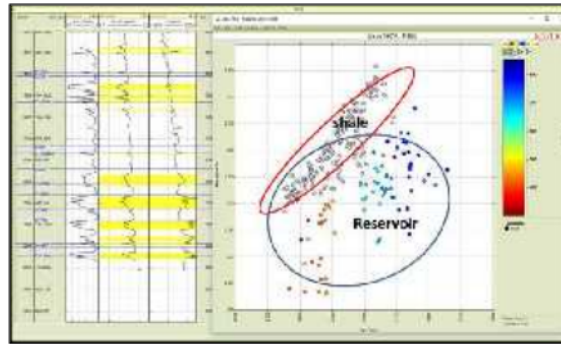
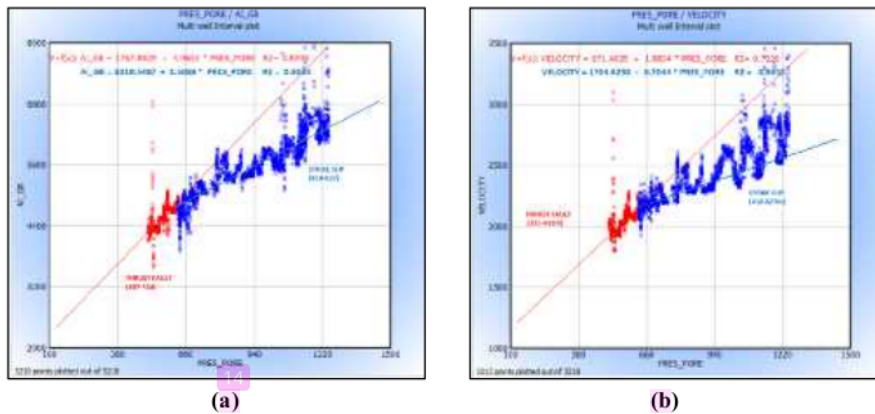


FIGURE 4. Crossplot between density and velocity which is the reservoir layer points are more scattered than shale layer points. The yellow interval shows reservoir layers.

Pore Pressure versus Acoustic Impedance

There is a separate trend between thrust-fault and strike-slip fault regime curves as a result of pore pressure and acoustic impedance relationship. This shows a non-linear state, particularly in the strike-slip fault regime and also implies an acoustic impedance value change which is not only controlled by pore pressure. Generally, pore pressure increases deeper along with hydrostatic gradient, despite the existence of separate trend between shale zone and reservoir. Therefore, the fluctuating acoustic impedance value is observed from the reservoir zone, instead of the relatively more stable shale zone. Furthermore, the V_p change of shale demonstrated more certainty compared to reservoir layers. This is evidently the different condition observed, when compared to the normal fault regime known as the alignment between loading state and decreasing porosity. Therefore, pore pressure accrual does not signify porosity increment directly in tectonic mechanism.



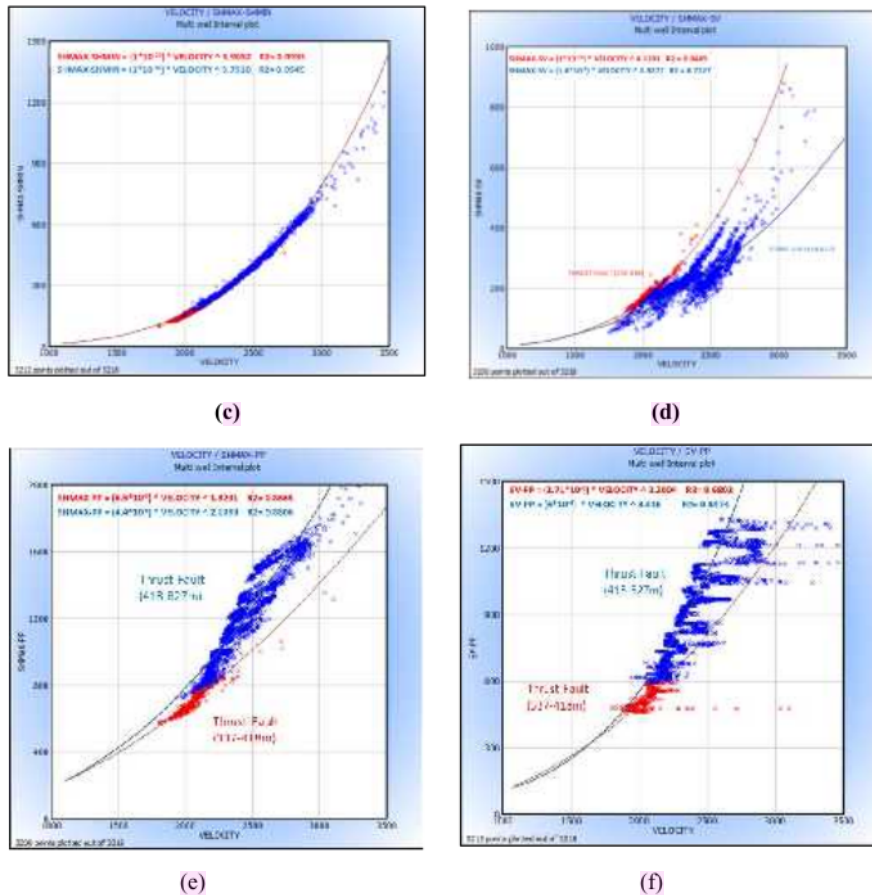


FIGURE 5. Some mechanical property cross-plots in terms to identify tectonic mechanism characteristics: (a) pore pressure vs acoustic impedance; (b) pore pressure vs velocity; (c) velocity vs $(S_H - S_{Hm})$; (d) velocity vs $(S_H - S_v)$; (e) velocity vs $(S_H - P_v)$; (f) velocity vs $(S_v - P_d)$.

Pore Pressure versus Velocity

Evidently, the shale and reservoir zone show a separate trend. Previous statement specified that the V_p certainty characteristic of both zones is higher compared to the density. The velocity change in the reservoir layers is not only caused by loading factors. These changes in the strike-slip fault regime are greater compared to the thrust fault regime. Meanwhile, the shale gradient in strike-slip is lesser compared to the thrust-fault regime.

Velocity versus $(S_H - S_{Hm})$

There are no separations between shale and reservoir layers, based on the relationship between velocity and the difference between S_H and S_{Hm} . The variation is characterized by an exponential curve with positive gradient. Also, no trend occurred between both regimes. This either indicates a proportional change between S_H and S_{Hm} , or shows the S_{Hm} as a lithology response due to the presence of S_H . However, for velocity above 3000 m/sec the change appears to be scattered due to tectonic regime change, as S_v value increases.

Velocity versus ($S_H - S_v$)

The certainty characteristic of the relationship between velocity and ($S_H - S_v$) is lower compared to ($S_H - S_{hm}$), as the nature of S_H and S_v are not interdependent. This indicates that the difference between S_H and S_v values are not sensitive to identify the effect of tectonic regimes to velocity.

Velocity versus ($S_H - P_p$)

Previous explanation stated that the pore pressure direction opposes the external stress acting on the medium. Therefore, the greater difference between external stresses and pore pressure influences the velocity. In addition, the greater difference between S_H and pore pressure shows the obtained curve is non-linear, but reveals a positive gradient and higher velocity. This situation occurs both for shale and reservoir as the velocity deviation range appeared in the strike-slip fault regime. Therefore, this indicates the external stresses influence beside S_H , and S_v is known to dominate as the second principal stress.

Velocity versus ($S_v - P_p$)

Recently, the surface condition is categorized as thrust fault regime. This assumes a deeper transformation to strike-slip, where S_v extends as the secondary principal stress. The appearance of the cross-plot curve shows the presence of a wide range of velocity values for S_v and pore pressure differences, especially in the reservoir layers. This does not occur in the shale layer, but demonstrates the effect of the difference between S_H and S_v is insignificant in fine-sized lithology such as impermeable shale, but rather considerable in the permeable reservoir rock. Therefore, the velocity tends to vary in ($S_v - P_p$) values.

Coupling Ratio ($\Delta S_h / \Delta P_p$)

The pore pressure changes (ΔP_p) and minimum horizontal stress changes (ΔS_{hm}) were combined during oil depletion as a result of pressure sequences occurring in sedimentary basins. This had been proved by separate periodic pore pressures. Subsequently, the Coulomb criterion was used to identify the pore pressure effect known to play a critical role in rock failure. The effective stress ($S_H - P_p$) controls the strength against shear failure rather than the total normal stress, and increasing pore pressure alone tend to induce failure in normal loading mechanism. The pore pressure depletion commonly associated with oil production possibly enhances stability by moving Mohr's circle to the right away from the failure envelope. Instead, pressure addition due to water injection is expected to displace Mohr's circle to the left. Therefore, the presence of total stress and pore pressure is combined, based on the concept of Terzaghi's effective stresses. Therefore, the coupling ratio $\Delta S_{hm} / \Delta P_p$ depends on the tectonic regime [34][35], apart from normal faulting and compaction. Poroelasticity is a possible pairing effect between P_p and S_{hm} [36], in terms of P_p interaction and S_{hm} reservoir stress path. This interaction is most common compared to the measured field data. For instance, S_{hm} is considered in hydrocarbon industry, and is determined by hydraulic fracturing or leak off tests.

Coupling ratio also shows the intensity of dynamic change on the rock deformation compared to pore pressure due to hydrocarbon exploitation and enhance oil recovery activities. The differential and deviatoric stresses are very important factors in the framework of related tectonic regime. For instance, the decrease in differential stress due to deviatoric change, results to a declining cohesion and friction angle. Also, the rock strength tend to reduce due to increasing differential stress. Furthermore, Z-600 reservoir zone was observed to be about 600 meters in depth and positioned in between thrust-fault and strike-slip regimes. The pore pressure recorded from 1994 - 2017 showed a decrease as a result of intensive oil production during 1994 - 2014, while an increase was reported from 2014 - 2017. This shows a tendency to lead to another factor besides loading. In order to observe the coupling ratio, the oil well P-404 was selected in the production and injection well networks. The picture below shows that the coupling ratio between P_p and S_{hm} is in the range of 0.3 - 0.4, and horizontal minimum stress change is lesser compared to pore pressure. This complies with the well condition where water has been injected since 2014. Based on table below, pore pressure appears to increase in line with S_H as S_v remains constant. Therefore, S_{hm} reflects the

lithology response to S_H and changes almost linearly to S_H changes. Moreover, S_{Hm} is known to extend beyond S_v .

The maximum and minimum values were selected for further observation. The maximum and minimum coupling ratios of 0.388 and 0.310 occurred at a depth of 642.36 m and 0.310, respectively. In addition, using Mohr diagram is intended to determine the variations in differential stress pattern on separate values of the coupling ratio, and to show a clear implications for rock strength. Principal stresses, σ_3 and σ_1 , were plotted in the Mohr diagram, after subtracting from pore pressure. Meanwhile, σ_3 in 1994 was specified as S_{Hm} , while σ_3 in 2017 denoted S_v , known to be relatively constant. This assumes a change occurred in the tectonic regime, specifically from the strike slip to the thrust fault regime. However, the S_{Hm} value increases almost in proportion to S_H . By using Mohr circle analysis, further observations were provided on the values as listed in the following table divided into initial and updated data from each depth with maximum and minimum values.

TABLE 1. The list of mechanical properties based on periodic pore pressure regarding to historical production matching (Well P-404).

DEPTH (m)	INITIAL YEAR (1994) in psi				UPDATED (2017) in psi				COUPLING RATIO		
	S_{Hmax}	S_{Hmin}	S_v	P_p	S_{Hmax}	S_{Hmin}	S_v	P_p	ΔS_{Hmax} (psi)	ΔP_p (psi)	$\Delta S_{Hmin} / \Delta P_p$
629.41	2170.67	1804.66	1908.26	947.96	2415.74	2066.04	1908.26	1723.17	261.38	775.21	0.34
630.02	2183.05	1801.24	1910.23	949.44	2417.71	2066.75	1910.23	1723.33	265.51	773.89	0.34
631.09	2159.87	1805.80	1913.65	951.85	2417.07	2069.99	1913.65	1731.35	264.19	779.50	0.34
633.07	2155.26	1807.11	1920.09	956.71	2402.84	2070.98	1920.09	1739.42	263.87	782.71	0.34
634.14	2189.13	1797.60	1923.41	958.52	2455.30	2088.62	1923.41	1744.47	291.02	785.94	0.37
635.05	2198.01	1798.75	1926.26	960.32	2453.71	2089.84	1926.26	1746.01	291.09	785.69	0.37
636.12	2188.81	1803.73	1929.60	963.34	2451.29	2064.94	1929.60	1748.47	261.22	785.13	0.33
637.49	2180.51	1823.47	1933.93	966.74	2469.44	2098.43	1933.93	1750.43	274.95	783.68	0.35
638.10	2197.66	1817.35	1935.87	968.26	2454.36	2095.36	1935.87	1751.30	278.01	783.04	0.36
639.32	2232.58	1819.69	1939.66	971.09	2467.26	2101.15	1939.66	1753.05	281.46	781.96	0.36
640.69	2287.65	1829.52	1944.00	974.74	2501.57	2113.04	1944.00	1754.87	283.52	780.13	0.36
641.15	2299.75	1829.05	1945.45	975.98	2518.51	2118.35	1945.45	1755.45	280.30	779.47	0.37
642.37	2316.64	1836.52	1949.29	978.73	2570.16	2134.11	1949.29	1756.95	297.59	778.22	0.38
643.13	2288.39	1822.53	1951.69	980.79	2576.71	2137.13	1951.69	1757.79	304.60	777.00	0.39
644.04	2294.26	1835.55	1954.54	983.29	2556.60	2133.51	1954.54	1758.64	297.97	775.36	0.38
645.11	2291.40	1842.50	1957.89	986.67	2552.86	2134.32	1957.89	1759.48	291.82	772.81	0.38
646.18	2305.91	1845.12	1961.30	990.46	2550.20	2135.41	1961.30	1760.27	290.29	769.81	0.38
647.40	2296.99	1845.53	1965.18	995.23	2565.67	2141.44	1965.18	1761.15	286.91	765.92	0.37
648.00	2313.03	1853.17	1967.14	997.45	2572.65	2144.24	1967.14	1761.55	291.07	764.10	0.38
649.07	2316.93	1860.89	1970.57	1001.43	2572.18	2145.38	1970.57	1760.48	284.49	759.05	0.37
650.75	2295.68	1863.07	1975.98	1007.81	2557.04	2141.03	1975.98	1750.25	277.96	742.43	0.37
651.05	2291.65	1865.22	1976.95	1008.91	2556.84	2140.85	1976.95	1748.18	275.63	739.27	0.37
652.12	2283.77	1868.91	1980.34	1012.34	2550.78	2140.02	1980.34	1744.32	271.11	731.97	0.37
653.95	2250.56	1878.69	1986.20	1017.68	2476.54	2121.81	1986.20	1737.80	243.12	720.12	0.34
654.41	2248.98	1893.70	1987.72	1018.72	2453.75	2114.11	1987.72	1728.62	220.41	709.90	0.31
656.39	2254.89	1890.02	1994.26	1022.92	2443.50	2107.64	1994.26	1702.16	217.62	679.24	0.32
657.30	2254.84	1886.86	1997.20	1024.32	2445.21	2106.62	1997.20	1690.96	219.76	666.64	0.33
658.06	2259.42	1886.01	1999.67	1025.74	2445.17	2106.14	1999.67	1684.53	220.13	658.79	0.33
659.43	2274.35	1879.84	2003.97	1026.35	2475.44	2115.28	2003.97	1683.02	235.43	656.67	0.36
660.04	2241.42	1911.19	2005.96	1026.92	2441.92	2108.24	2005.96	1684.06	197.05	657.15	0.30

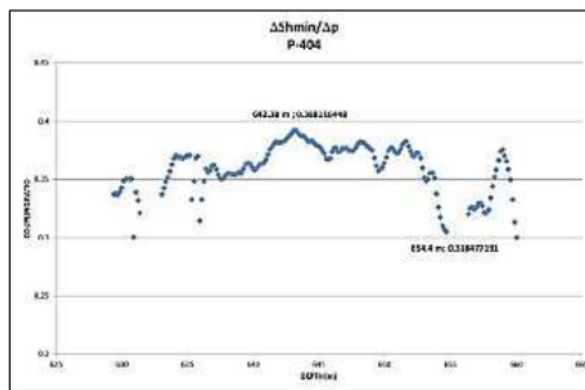


FIGURE 6. Coupling ratio values present in the interval of Z-600 as observed from Well P-404.

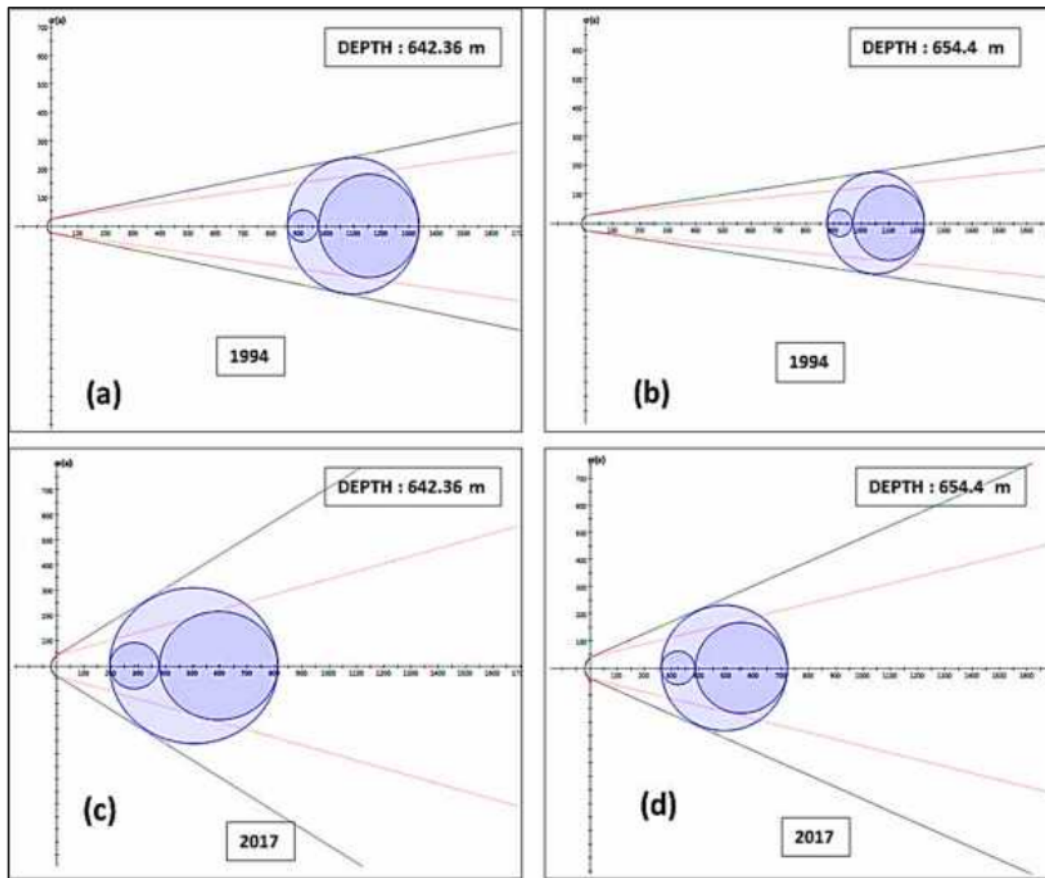


FIGURE 7. Mohr diagram of: (a) initial Z-600 mechanical properties at depth 642.36 m; (b) initial Z-600 mechanical properties at depth 654.4 m; (c) after updated Z-600 mechanical properties at depth 642.36 m; (d) after updated Z-600 mechanical properties at depth 654.4 m (as observed from Well P-404).

DISCUSSION

Mohr diagram analysis was conducted to describe the impact of pore pressure corresponding to an increase in S_H and S_{Nm} . The enhanced pore pressure commonly reduces the effective stresses, but conducts shear failure in this study. Figure 7a and 7b show the Z-600 reservoir with similar cohesion value 25 kPa, but lower friction angle 8.30 in the deeper layer (654.4 m), while lower depth (642.35 m) estimates 11.350. Subsequently, with the update in historical production from 1994 - 2017, the cohesion value and friction angle reflected 40 kPa and 340, respectively for a depth of 642.35 m. Meanwhile, the values were reported as 38 kPa and 240, correspondingly at a depth of 654.4 m, (Figure 7c and Figure 7d). Therefore, increasing both pore pressure and horizontal stresses possibly enhances rock strength.

The aforementioned condition serves as reference material to conduct further evaluation on the effect of effective stresses on the relationship of pore pressure and velocity. In this case, the matrix bound structure is expected to influence the velocity. This is illustrated for more details, commencing with the basic concept of understanding as illustrated by Figure 8. Under this situation, vertical stress (S_v) appears as a cumulative of normal tensor components working vertically, and also as a gravity manifestation at each point without shear stresses. Hence, normal tensor components are always vertically downward, and are controlled by pore pressure.

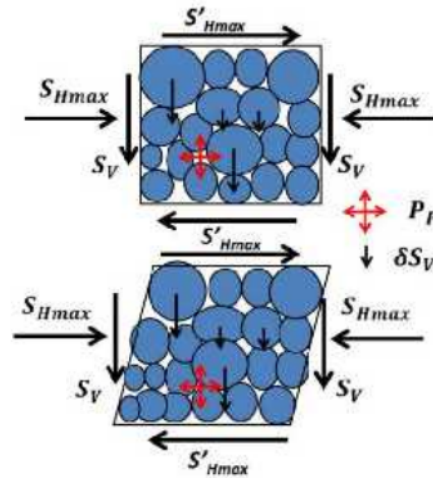


FIGURE 8. The schematic diagram of principal stresses and pore pressure.

As the pore pressure declines in the normal fault regime, the normal tensor components control the available space resulting to the pore closing. This also occurs in both regimes provided S_v is not the primary principal stress. However, the influence is not in the normal fault regime, but maximum horizontal stress is the primary stress in this circumstance. S_H is a set of normal and shear tensor components known to act on sediment matrices. The normal tensor is nearby inter-granules and the shear tensor shifts over the grain surfaces. Hence, the pore pressure then counter-attacks the normal tensor of horizontal stresses. Furthermore, a shear failure was evident due to pore pressure involvement. The pore pressure components possess similar direction with shear tensor of horizontal stresses. Consequently, the granules tend to shift and break away and the grain size as well as the sortation pattern demonstrates each various responses as observed from the cross plot of pore pressure and velocity (Figure 5b). Sand is uncertain rather than shale. Therefore, it appears the trend is not able to distinguish the tectonic regimes, but the shale, however, shows the capacity to separate these matter. Based on the effective stresses known as the difference between principal stress and pore pressure, it is observed that the most influential stress components are horizontal stresses (S_H and S_{hm}) due to the direct relationship between the S_H and S_{hm} variation with velocity (Figure 5c and 5e). Meanwhile, the difference between S_H and S_v does not have any direct correspondence (Figure 5d and 5f), as it cannot be considered scalarly as shown in Figure 8. Therefore, velocity depends on the differential stress between S_H and S_{hm} , and the coupling ratio ($\Delta S_{hm} / \Delta P_p$) at approximately 0.3, produces an increasing velocity, despite the tendency of a shear tensile failure to occur potentially due to intensive water injection activities.

CONCLUSIONS

Based on above discussion, we can summarize several points:

- The effective stresses depend not only on pore pressure, but also on differential or deviatoric stress. Hence, these are unlikely to be alienated from the state of tectonic regimes.
- Increased pore pressure tends to diminish the rock strength as the differential stress value decreases such as occurred in loading mechanism. However, there is an enhanced differential stress in the tectonic mechanism, particularly thrust-fault regime, where the primary principal stress is S_H and the least principal stress is S_v .

- As pore pressure and differential stress increase, the velocity possibly rises. This possibly occurs in tectonic mechanism.

ACKNOWLEDGMENT

The authors would like to acknowledge PT. Pertamina EP, which permitting their data to be studied. We also would like to thank to Dr. Ir. Muhammad Burhannuddinur, M.Sc as Dean of Faculty of Earth Technology and Energy, Universitas Trisakti, for a lot of support. Last but not least, we would like to thank to our colleagues Amalia Nurani, Rischia Jayanti and Aris Endartyanto in PT. Elmusa Tbk for their valuable assistance.

REFERENCES

- [1] E. Detournay, and A.H.D. Cheng. Fundamentals of poroelasticity, Pergamon Press, 113-171, 1993.
- [2] R. Yoshinaka, T.V. Tran, and M. Osada. Pore pressure changes and strength mobilization of soft rocks in consolidated-undrained cyclic loading triaxial tests, *Int. J. Rock Mech. Min. Sci.* 34 5, 715-726, 1997.
- [3] I. Yilmaz . Influence of water content on the strength and deformability of gypsum, *Int. J. Rock Mech. Min. Sci.* 42 2, 342-347, 2010.
- [4] M.S.A. Perera, P.G. Ranjith, and M. Peter. Effect of saturation medium and pressure on strength parameters of Latrobe Valley brown coal: Carbon dioxide, water and nitrogen saturations, *Energy* 36 12 6941-6947, 2011.
- [5] D. Li, L.N.Y. Wong, G. Liu, and X. Zhang. Influence of water content and anisotropy on the strength and deformability of low porosity metasedimentary rocks under triaxial compression, *Eng Geol.* 126, 46-66, 2012.
- [6] A. Kumar. The effect of stress rate and temperature on the strength of basalt and granite, *Geophysics* 33 3, 501-510, 1968.
- [7] J.C. Jaeger, and N.G.W. Cook. Fundamentals of Rock Mechanics, Chapman and Hall London, 1979.
- [8] I.W. Farmer, Engineering Behavior of Rock, Chapman and Hall London, 1983.
- [9] N.D. Cristescu, and U. Hunsche, Time Effects in Rock mechanics, John Wiley and Sons New York, 1998.
- [10] G.Z. Ugwu. An overview of pore pressure prediction using seismically-derived velocities, *Journal of Geology and Mining Research* 7 4, 31-40, 2015.
- [11] J. Sun, and Y.Y. Hu. Time-dependent effects on the tensile strength of saturated granite at three gorges project in China, *Int. J. Rock Mech. Min. Sci.* 34 3-4, 306.e1-306.e13, 1997.
- [12] K. Masuda. Effects of water on rock strength in a brittle regime, *J. Struct. Geol.* 23 11, 1653-1657, 2001.
- [13] B. Vasarhelyi. Some observations regarding the strength and deformability of sandstones in case of dry and saturated conditions, *Bull., Eng., Geol., Env.*, 62, 245-249, 2003.
- [14] A. Torok , and B. Vasarhelyi. The influence of fabric and water content on selected rock mechanical parameters of travertine, examples, Hungary *Eng. Geol.* 115, 237-245, 2010.
- [15] B.A. Eaton. The equation for geopressure prediction from well logs, *Soc. Petr. Engineers*, 5544, 1975.
- [16] K. Terzaghi. Theoretical soil mechanics. John Wiley and Sons, Inc., 1943.
- [17] J.G. Sclater, and P.A.F. Christie. Continental stretching: An explanation of the Post-Mid-Cretaceous subsidence of the central, North Sea Basin *J. Geophys. Res.* 85, 3711-3739, 1980.
- [18] S. Hansen . A compaction trend for Cretaceous and Tertiary shales on the Norwegian Shelf based on sonic transit times, *Petrol. Geosci.* 12, 159-166, 1996.
- [19] J.W. Schmoker, and D.I. Gautier. Compaction of Basin sediments: Modelling based on time temperature history, *J. Geophys. Res.* 94(B6), 7379-7386, 1989.
- [20] J.B. Burland. On the compressibility and shear strength of natural clays, *Geotechnique* 40 , 329-378, 1990.
- [21] Y. Yang , and A.C. Aplin. Definition and practical application of mudstone porosity-effective stress relationships, *Petrol. Geosci.* 10, 153-162, 2004.
- [22] G.L. Bowers. Pore pressure estimation from velocity data: accounting for overpressure mechanisms besides undercompaction, *SPE Drilling and completions*, 89-95, 1995.

- [23] I. Shahab, I. Suhartanto, R.R. Wathan, and M.D. Junaidi, Reaktivasi shallow zone dalam upaya pencarian sisa-sisa dan peningkatan produksi minyak di Struktur Rantau. Prosiding IATMI Bandung, pp. 1-10, 2005.
- [24] H. Darman, and F.H. Sidi. An outline of the geology of Indonesia, IAGI. 17-22, 2000.
- [25] J.D. Bennett, D.McC.Bridge, N.R.C. Cameron, A. Djaenuddin, S.A. Ghazali, D.H. Jeffrey, W. Kartawa, W. Keats. N.M.S. Rock, and S.J. Thompson. Geologi Lembar Langsa, Sumatera (The Geology of the Langsa Quadrangle, Sumatera), Pusat Penelitian dan Pengembangan Geologi Direktorat Jenderal Pertambangan Umum Departemen Pertambangan dan Energi, 1985.
- [26] I.S. Ronoatmojo, G.S. Titaley, A. Widiyanto, W. Silvia, A. Nurani, and R. Jayanti. The case study of empirical relation between pore pressure and P-impedance in shallow layer, JCM HAGI - IAGI - IAFMI-IATMI, 1-4, 2017.
- [27] I.A. Garagash, A.V. Dubovskaya, D.A. Korneva, M. Ghasemi, and Gubkin. Coupled geomechanical and fluid flow simulation of the oil field evolution induced by reservoir production, SPE Russian Oil and Gas Exploration and Production Technical Conference and Exhibition, Moscow (Russia) 14 - 16 October 2014 SPE-171215-MS, 1-10, 2014.
- [28] R.W. Lewis, and Y. Sukirman. Finite different modeling of three-phase flow in deforming saturated oil reservoirs *International Journal for Numerical and Analytical Methods in Geomechanics* 8, 577-598, 1993.
- [29] R.W. Lewis, and H.R. Ghafouri. A novel finite element double porosity model for multiphase flow through deformable fractured porous media, *International Journal for Numerical and Analytical Methods in Geomechanics* 11, 789-816, 1997.
- [30] S.E. Minkoff, C.M. Stone, S. Bryant, M. Peszyńska, and M.F. Wheeler. Coupled fluid flow and geomechanical deformation modeling *Journal of Petroleum Science and Engineering* 38, 37-56, 2003.
- [31] J.G. Osorio, H.Y. Chen, and L.W. Teufel. Numerical simulation of the impact of flow induced geomechanical response on the productivity of the stress-sensitive reservoir SPE Reservoir Simulation Symposium held in Houston, 1999.
- [32] A.F. Rahman, A. Haris, and I.S. Ronoatmojo. Determining the reservoir compartments based on fault sealing analysis studying of Tamiang field North Sumatera Basin, Indonesia, AIP Conference Proceeding 2023 020262 (2018), 1-5, 2018
- [33] I.S. Ronoatmojo, G.S. Titaley, A. Widiyanto, W. Silvia, A. Nurani, and R. Jayanti. The case study of empirical relation between pore pressure and P-impedance in shallow layer, JCM HAGI - IAGI - IAFMI-IATMI, 1-4, 2017.
- [34] M.A. Addis. The stress-depletion response of reservoirs. Society of Petroleum Engineers. SPE 38720, 55-65, 1997.
- [35] R. Hillis. Pore pressure/stress coupling and its implications for seismicity, *Exploration Geophysics* 31, 448-454, 2000.
- [36] N.R. Gouly. Reservoir stress path during depletion of Norwegian chalk oilfields, *Petroleum Geoscience* 9, 233-241, 2003.

The effect

ORIGINALITY REPORT

34%
SIMILARITY INDEX

30%
INTERNET SOURCES

33%
PUBLICATIONS

12%
STUDENT PAPERS

PRIMARY SOURCES

1 pubs.aip.org **16%**
Internet Source

2 Submitted to School of Business and Management ITB **3%**
Student Paper

3 aip.scitation.org **3%**
Internet Source

4 academicjournals.org **2%**
Internet Source

5 watermark.silverchair.com **1%**
Internet Source

6 www.mines.edu **1%**
Internet Source

7 www.researchgate.net **1%**
Internet Source

8 Z Ugwu G. "An overview of pore pressure prediction using seismically derived velocities", Journal of Geology and Mining Research, 2015 **1%**
Publication

9	R. Hillis. "Pore pressure/stress coupling and its implications for seismicity", Exploration Geophysics, 2000 Publication	1 %
10	ifory.id Internet Source	1 %
11	Ugwu, G Z. "Pore pressure prediction using seismic data: Insight from Onshore Niger Delta, Nigeria", Journal of Geology and Mining Research, 2015. Publication	1 %
12	idoc.pub Internet Source	<1 %
13	maxwellsci.com Internet Source	<1 %
14	www.hindawi.com Internet Source	<1 %
15	Altmann, Johannes Benedikt. "Poroelastic effects in reservoir modelling", Universität Karlsruhe, 2010. Publication	<1 %
16	mining.eng.cmu.ac.th Internet Source	<1 %
17	pure.kfupm.edu.sa Internet Source	<1 %

18

Imam Setiaji Ronoatmojo, Muhamad Burhannudinnur, Hidartan, Grace Stephani Titaley. "The identification of tectonic regimes based on mechanical properties derived from log data in Nangroe Aceh Darussalam", AIP Publishing, 2021

Publication

<1 %

19

Thomas Hantschel. "Pore Pressure, Compaction and Tectonics", Fundamentals of Basin and Petroleum Systems Modeling, 2009

Publication

<1 %

20

www.karyailmiah.trisakti.ac.id

Internet Source

<1 %

21

Ahmad Pouya, Irini Djéran-Maigre, Violaine Lamoureux-Var, Daniel Grunberger. "Mechanical behaviour of fine grained sediments: experimental compaction and three-dimensional constitutive model", Marine and Petroleum Geology, 1998

Publication

<1 %

22

C. M. Aruffo, A. Rodriguez-herrera, E. Tenthorey, F. Krzikalla, J. Minton, A. Henk. "Geomechanical modelling to assess fault integrity at the CO2CRC Otway Project, Australia", Australian Journal of Earth Sciences, 2014

Publication

<1 %

23

gfzpublic.gfz-potsdam.de

Internet Source

<1 %

24

Jean-Claude Roegiers. "Rock Mechanics as a Multidisciplinary Science - Proceedings of the 32nd U.S. Symposium", A.A. Balkema, Rotterdam, 2020

Publication

<1 %

25

Xiang Li, Heinz Konietzky. "Numerical simulation schemes for time-dependent crack growth in hard brittle rock", Acta Geotechnica, 2014

Publication

<1 %

26

idoc.tips

Internet Source

<1 %

27

Keith Hawkins. "High resolution pore-pressure prediction from AVO derived velocities; a North Sea case study", SEG Technical Program Expanded Abstracts, 1999

Publication

<1 %

28

Liu, Rui, Jianzhang Liu, Weilin Zhu, Fang Hao, Yuhong Xie, Zhengfeng Wang, and Lifeng Wang. "In situ stress analysis in the Yinggehai Basin, northwestern South China Sea: Implication for the pore pressure-stress coupling process", Marine and Petroleum Geology, 2016.

Publication

<1 %

29	pg.lyellcollection.org Internet Source	<1 %
30	www.j3.jstage.jst.go.jp Internet Source	<1 %
31	www.scribd.com Internet Source	<1 %
32	G.N. Pande, S. Pietruszczak, H.F. Schweiger. "Numerical Models in Geomechanics", Taylor and Francis, 2020 Publication	<1 %
33	Hans-Peter Rossmannith. "Mechanics of Jointed and Faulted Rock", CRC Press, 2018 Publication	<1 %
34	Yin, Shuai, Wenlong Ding, Wen Zhou, Yuming Shan, Runcheng Xie, Chunhua Guo, Xiangyu Cao, Ruyue Wang, and Xinghua Wang. "In situ stress field evaluation of deep marine tight sandstone oil reservoir: A case study of Silurian strata in northern Tazhong area, Tarim Basin, NW China", Marine and Petroleum Geology, 2017. Publication	<1 %
35	Amirlatifi, Amin. "Coupled geomechanical reservoir simulation.", Proquest, 2014. Publication	<1 %

36

Imam Setiaji Ronoatmojo, Muhamad Burhannudinnur, Grace Stephani Titaley. "The influence of tectonic forces on the coupling ratio of sand Z-600, Keutapang formation, North Sumatra Basin", AIP Publishing, 2020

Publication

<1 %

Exclude quotes Off

Exclude matches Off

Exclude bibliography Off